



# TECH BRIEFS

NATIONAL AERONAUTICS AND SPACE ADMINISTRATION

-  **Technology Focus**
-  **Electronics/Computers**
-  **Software**
-  **Materials**
-  **Mechanics/Machinery**
-  **Manufacturing**
-  **Bio-Medical**
-  **Physical Sciences**
-  **Information Sciences**
-  **Books and Reports**



## INTRODUCTION

Tech Briefs are short announcements of innovations originating from research and development activities of the National Aeronautics and Space Administration. They emphasize information considered likely to be transferable across industrial, regional, or disciplinary lines and are issued to encourage commercial application.

### Availability of NASA Tech Briefs and TSPs

Requests for individual Tech Briefs or for Technical Support Packages (TSPs) announced herein should be addressed to

#### National Technology Transfer Center

Telephone No. (800) 678-6882 or via World Wide Web at [www.nttc.edu](http://www.nttc.edu)

Please reference the control numbers appearing at the end of each Tech Brief. Information on NASA's Innovative Partnerships Program (IPP), its documents, and services is also available at the same facility or on the World Wide Web at <http://www.nasa.gov/offices/ipp/network/index.html>

Innovative Partnerships Offices are located at NASA field centers to provide technology-transfer access to industrial users. Inquiries can be made by contacting NASA field centers listed below.

## NASA Field Centers and Program Offices

#### Ames Research Center

Lisa L. Lockyer  
(650) 604-1754  
[lisa.l.lockyer@nasa.gov](mailto:lisa.l.lockyer@nasa.gov)

#### Dryden Flight Research Center

Gregory Poteat  
(661) 276-3872  
[greg.poteat@dfrc.nasa.gov](mailto:greg.poteat@dfrc.nasa.gov)

#### Glenn Research Center

Kathy Needham  
(216) 433-2802  
[kathleen.k.needham@nasa.gov](mailto:kathleen.k.needham@nasa.gov)

#### Goddard Space Flight Center

Nona Cheeks  
(301) 286-5810  
[nona.k.cheeks@nasa.gov](mailto:nona.k.cheeks@nasa.gov)

#### Jet Propulsion Laboratory

Andrew Gray  
(818) 354-3821  
[gray@jpl.nasa.gov](mailto:gray@jpl.nasa.gov)

#### Johnson Space Center

information  
(281) 483-3809  
[jsc.techtran@mail.nasa.gov](mailto:jsc.techtran@mail.nasa.gov)

#### Kennedy Space Center

David R. Makufka  
(321) 867-6227  
[david.r.makufka@nasa.gov](mailto:david.r.makufka@nasa.gov)

#### Langley Research Center

Brian Beaton  
(757) 864-2192  
[brian.f.beaton@nasa.gov](mailto:brian.f.beaton@nasa.gov)

#### Marshall Space Flight Center

Jim Dowdy  
(256) 544-7604  
[jim.dowdy@msfc.nasa.gov](mailto:jim.dowdy@msfc.nasa.gov)

#### Stennis Space Center

Ramona Travis  
(228) 688-3832  
[ramona.e.travis@nasa.gov](mailto:ramona.e.travis@nasa.gov)

#### Carl Ray, Program Executive

Small Business Innovation  
Research (SBIR) & Small  
Business Technology  
Transfer (STTR) Programs  
(202) 358-4652  
[carl.g.ray@nasa.gov](mailto:carl.g.ray@nasa.gov)

#### Doug Comstock, Director

Innovative Partnerships  
Program Office  
(202) 358-2560  
[doug.comstock@nasa.gov](mailto:doug.comstock@nasa.gov)





# TECH BRIEFS

NATIONAL AERONAUTICS AND SPACE ADMINISTRATION



## 5 Technology Focus: Test & Measurement

- 5 Insulation-Testing Cryostat With Lifting Mechanism
- 6 Optical Testing of Retroreflectors for Cryogenic Applications
- 6 Measuring Cyclic Error in Laser Heterodyne Interferometers
- 7 Self-Referencing Hartmann Test for Large-Aperture Telescopes
- 8 Measuring a Fiber-Optic Delay Line Using a Mode-Locked Laser



## 9 Electronics/Computers

- 9 Reconfigurable Hardware for Compressing Hyperspectral Image Data
- 9 Spatio-Temporal Equalizer for a Receiving-Antenna Feed Array
- 10 High-Speed Ring Bus
- 11 Nanoionics-Based Switches for Radio-Frequency Applications
- 12 Lunar Dust-Tolerant Electrical Connector
- 12 Compact, Reliable EEPROM Controller
- 13 Quad-Chip Double-Balanced Frequency Tripler
- 13 Ka-Band Waveguide Two-Way Hybrid Combiner for MMIC Amplifiers
- 14 Radiation-Hardened Solid-State Drive



## 15 Manufacturing & Prototyping

- 15 Use of Nanofibers to Strengthen Hydrogels of Silica, Other Oxides, and Aerogels
- 15 Two Concepts for Deployable Trusses



## 17 Mechanics/Machinery

- 17 Concentric Nested Toroidal Inflatable Structures
- 18 Investigating Dynamics of Eccentricity in Turbomachines



## 19 Materials

- 19 Improved Low-Temperature Performance of Li-Ion Cells Using New Electrolytes



## 21 Physical Sciences

- 21 Integrity Monitoring of Mercury Discharge Lamps
- 21 White-Light Phase-Conjugate Mirrors as Distortion Correctors
- 22 Biasable, Balanced, Fundamental Submillimeter Monolithic Membrane Mixer



## 23 Software

- 23 ICER-3D Hyperspectral Image Compression Software
- 23 Context Modeler for Wavelet Compression of Spectral Hyperspectral Images

This document was prepared under the sponsorship of the National Aeronautics and Space Administration. Neither the United States Government nor any person acting on behalf of the United States Government assumes any liability resulting from the use of the information contained in this document, or warrants that such use will be free from privately owned rights.





## Insulation-Testing Cryostat With Lifting Mechanism

Cryogenic-insulation specimens can be tested reliably under typical conditions of use.

John F. Kennedy Space Center, Florida

The figure depicts selected aspects of an apparatus for testing thermal-insulation materials for cryogenic systems at temperatures and under vacuum or atmospheric conditions representative of those encountered in use. This apparatus, called “Cryostat-100,” is based on the established cryogen-boil-off calorimeter method, according to which the amount of heat that passes through an insulation specimen to a cryogenic fluid in a container, and thus the effective thermal conductance of the specimen, is taken to be proportional to the amount of the cryogenic fluid that boils off from the container.

The design of Cryostat-100 is based partly on, and incorporates improvements over, the design of a similar prior apparatus called “Cryostat-1” described in “Improved Methods of Testing Cryogenic Insulation Materials” (KSC-12107 & KSC-12108), *NASA Tech Briefs*, Vol. 24, No. 12 (December 2000), page 46. The design of Cryostat-100 also incorporates the best features of two other similar prior apparatuses called “Cryostat-2” (also described in the cited prior article) and “Cryostat-4.” Notable among the improvements in Cryostat-100 is the addition of a lifting mechanism that enables safe, rapid, reliable insertion and removal of insulation specimens and facilitates maintenance operations that involve lifting.

As in Cryostat-1, the cold mass is a vertical stainless-steel cylindrical vessel subdivided into a larger measurement vessel with smaller thermal-guard vessels at both ends. During operation, all three vessels are kept filled with liquid nitrogen near saturation at ambient pressure (temperature  $\approx 77.4$  K). The cold mass of Cryostat-100 has a length of 1 m and diameter of 168 mm. Each specimen has a corresponding nominal length and inner diameter and a nominal thickness of 25.4 mm. Specimens that are shorter and have thicknesses between 0 and 50 mm are also acceptable. Bulk-fill, foam, clam-shell, multilayer insulation, and layered materials can be tested over a very wide range of thermal transmission: apparent thermal conductivity from 0.01

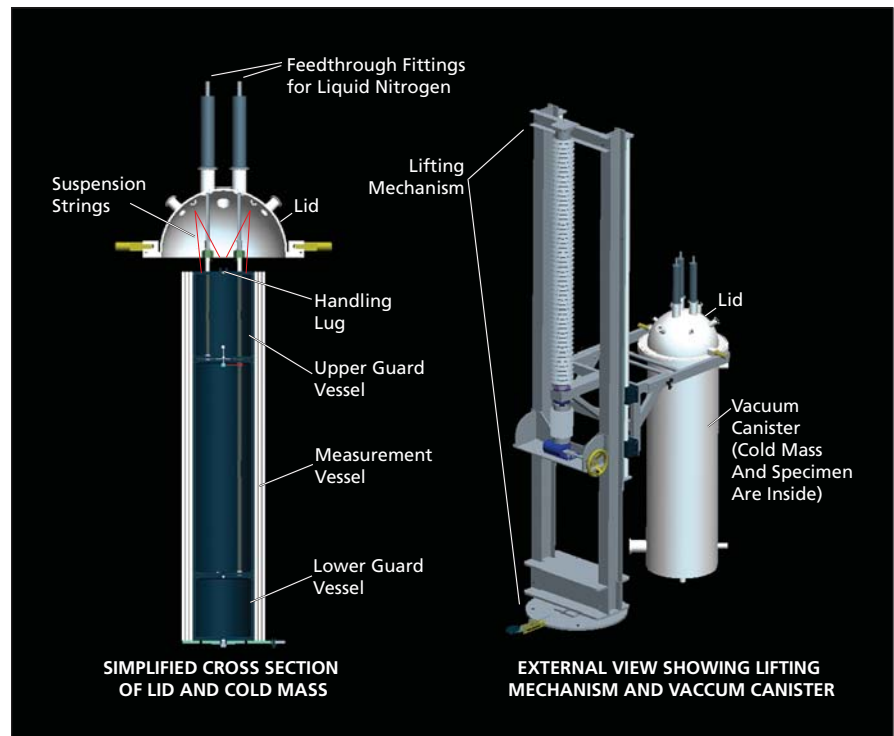
to 60 mW/m-K and heat flux from 0.1 to 500 W/m<sup>2</sup>.

A test in Cryostat-100 can be conducted at any desired gas pressure between ambient atmospheric pressure at one extreme and a vacuum with residual pressure  $<10^{-5}$  torr ( $<1.33 \times 10^{-3}$  Pa) at the other extreme. The residual gas (and purge gas) is typically nitrogen, but can be any suitable purge gas (e.g., helium, argon, or carbon dioxide). Usually, the temperature on the warm boundary of the insulation specimen is maintained near the ambient value (approximately 293 K), while the boiling of liquid nitrogen at atmospheric pressure in the cold mass maintains the temperature on the cold boundary of the specimen at approximately 77 K.

Much less ancillary equipment is needed for proper operation of Cryostat-100 than is needed for the prior apparatus: Unlike Cryostat-1, Cryostat-100 is not connected to a storage tank, phase separator, or subcooler. Cryostat-100 has

a top-loading configuration that makes it possible to perform convenient assembly, disassembly, insertion and removal of specimens, and connection and disconnection of instrumentation. The degree of thermal stability of Cryostat-100 is much improved because of the incorporation of internal vapor plates, a single-tube system for filling and venting, bellows feedthroughs, string suspension of the cold mass within the vacuum canister, and heavy-wall stainless-steel construction. Other features that contribute to reliability and efficiency in all phases of test procedures include guide rings, handling tools, and material installation fixtures.

*This work was done by James Fesmire, Adam Dokos, and Brekke Scholtens of Kennedy Space Center and Zoltan Nagy and Stanislaw Augustynowicz of Sierra Lobo, Inc. For further information, contact the Kennedy Innovative Partnerships Program Office at (321) 861-7158. KSC-13047*



Cryostat-100 incorporates improvements over similar prior apparatuses that make it possible to perform test and maintenance operations faster and more easily and to better ensure the reliability of test data.

## Optical Testing of Retroreflectors for Cryogenic Applications

Commercial uses include cryogenic metrology on aerospace structures and optical metrology instrumentation.

Goddard Space Flight Center, Greenbelt, Maryland

A laser tracker (LT) is an important coordinate metrology tool that uses laser interferometry to determine precise distances to objects, points, or surfaces defined by an optical reference, such as a retroreflector. A retroreflector is a precision optic consisting of three orthogonal faces that returns an incident laser beam nearly exactly parallel to the incident beam. Commercial retroreflectors are designed for operation at room temperature and are specified by the divergence, or beam deviation, of the returning laser beam, usually a few arcseconds or less. When a retroreflector goes to extreme cold ( $\approx 35$  K), however, it could be anticipated that the precision alignment between the three faces and the surface

figure of each face would be compromised, resulting in wavefront errors and beam divergence, degrading the accuracy of the LT position determination.

Controlled tests must be done beforehand to determine survivability and these LT coordinate errors. Since conventional interferometer systems and laser trackers do not operate in vacuum or at cold temperatures, measurements must be done through a vacuum window, and care must be taken to ensure window-induced errors are negligible, or can be subtracted out. Retroreflector holders must be carefully designed to minimize thermally induced stresses. Changes in the path length and refractive index of the retroreflector have to be considered.

Cryogenic vacuum testing was done on commercial solid glass retroreflectors for use on cryogenic metrology tasks. The capabilities to measure wavefront errors, measure beam deviations, and acquire laser tracker coordinate data were demonstrated. Measurable but relatively small increases in beam deviation were shown, and further tests are planned to make an accurate determination of coordinate errors.

*This work was done by Raymond G. Ohl and Bradley J. Frey of Goddard Space Flight Center, Joseph M. Stock of SGT, Inc., Joseph C. McMann of QinetiQ-North America, and Tmitri J. Zukowski of Research Support Instruments. For further information, contact the Goddard Innovative Partnerships Office at (301) 286-5810. GSC-15702-1*

## Measuring Cyclic Error in Laser Heterodyne Interferometers

Amplitude modulation, instead of phase modulation, associated with displacement oscillations is measured.

NASA's Jet Propulsion Laboratory, Pasadena, California

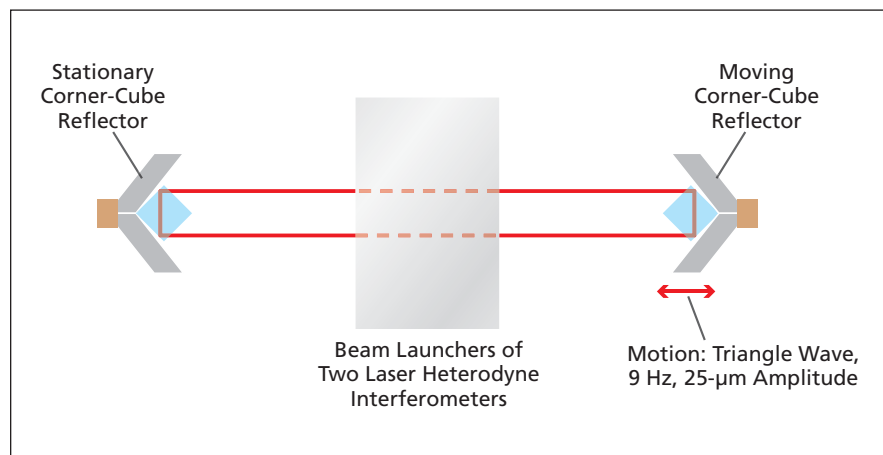
An improved method and apparatus have been devised for measuring cyclic errors in the readouts of laser heterodyne interferometers that are configured and operated as displacement gauges. The cyclic errors arise as a consequence of mixing of spurious optical and electrical signals in beam launchers that are subsystems of such interferometers. The conventional approach to measurement of cyclic error involves phase measurements and yields values precise to within about 10 pm over air optical paths at laser wavelengths in the visible and near infrared. The present approach, which involves amplitude measurements instead of phase measurements, yields values precise to about  $\approx 0.1$  pm — about 100 times the precision of the conventional approach.

In a displacement gauge of the type of interest here, the laser heterodyne interferometer is used to measure any change in distance along an optical axis between two corner-cube retroreflectors. One of the corner-cube retroreflectors is mounted on a piezoelectric transducer (see figure), which is used to

introduce a low-frequency periodic displacement that can be measured by the gauges. The transducer is excited at a frequency of 9 Hz by a triangular waveform to generate a 9-Hz triangular-wave displacement having an amplitude of 25  $\mu\text{m}$ .

The displacement gives rise to both amplitude and phase modulation of the heterodyne signals in the gauges.

The modulation includes cyclic error components, and the magnitude of the cyclic-error component of the phase modulation is what one needs to measure in order to determine the magnitude of the cyclic displacement error. The precision attainable in the conventional (phase measurement) approach to measuring cyclic error is limited because the phase measurements are af-



**Displacement Oscillations** are introduced between two corner-cube retroreflectors that are common to two displacement gauges. The magnitude of an amplitude modulation in the outputs of the gauges is measured.

ected by phase noise contributed mainly by vibrations and air turbulence. However, the amplitude modulation associated with the cyclic phase error is not affected by vibrations and air turbulence.

Therefore, in the present approach, in order to achieve higher precision in measuring cyclic error, one measures

the amplitude modulation instead of the phase modulation. The heterodyne error signal is fed to a relatively simple demodulator circuit, which removes the radio-frequency component of the heterodyne error signal, leaving only the 9-Hz amplitude modulation. The output of the demodulator is fed to a spectrum analyzer or an oscilloscope for measure-

ment of the magnitude of the 9-Hz amplitude modulation.

*This work was done by Daniel Ryan, Alexander Abramovici, Feng Zhao, Frank Dekens, Xin An, Alireza Azizi, Jacob Chap-sky, and Peter Halverson of Caltech for NASA's Jet Propulsion Laboratory. Further information is contained in a TSP (see page 1). NPO-45157*

## Self-Referencing Hartmann Test for Large-Aperture Telescopes

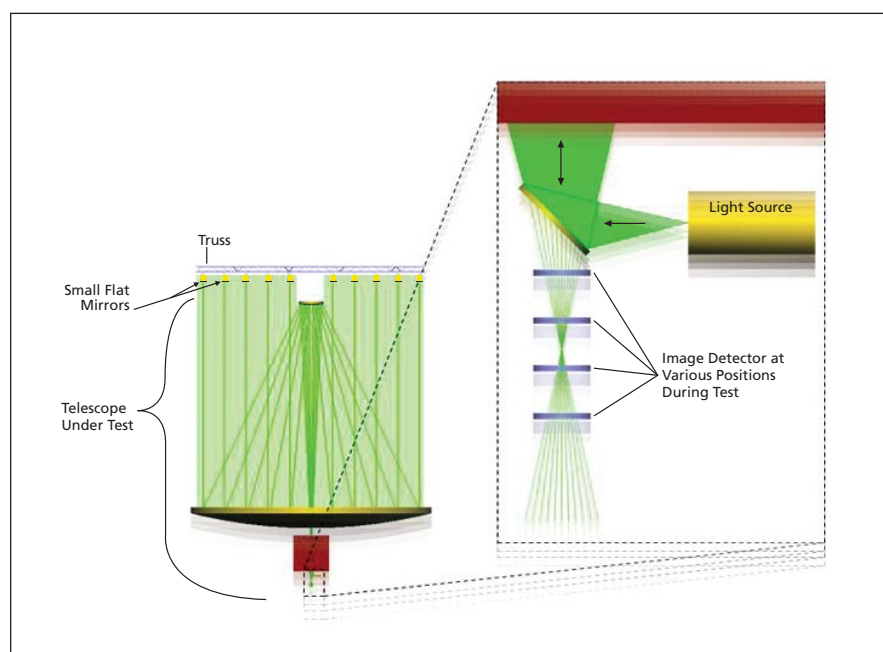
**Full aperture testing of large-aperture telescopes is performed without the need for an equally large-aperture autocollimating flat.**

*NASA's Jet Propulsion Laboratory, Pasadena, California*

A method is proposed for end-to-end, full aperture testing of large-aperture telescopes using an innovative variation of a Hartmann mask. This technique is practical for telescopes with primary mirrors tens of meters in diameter and of any design. Furthermore, it is applicable to the entire optical band (near IR, visible, ultraviolet), relatively insensitive to environmental perturbations, and is suitable for ambient laboratory as well as thermal-vacuum environments. The only restriction is that the telescope optical axis must be parallel to the local gravity vector during testing.

The standard Hartmann test utilizes an array of pencil beams that are cut out of a well-corrected wavefront using a mask. The pencil beam array is expanded to fill the full aperture of the telescope. The detector plane of the telescope is translated back and forth along the optical axis in the vicinity of the nominal focal plane, and the centroid of each pencil beam image is recorded. Standard analytical techniques are then used to reconstruct the telescope wavefront from the centroid data. The expansion of the array of pencil beams is usually accomplished by double passing the beams through the telescope under test. However, this requires a well-corrected, autocollimation flat, the diameter or which is approximately equal to that of the telescope aperture. Thus, the standard Hartmann method does not scale well because of the difficulty and expense of building and mounting a well-corrected, large aperture flat.

The innovation in the testing method proposed here is to replace the large aperture, well-corrected, monolithic autocollimation flat with an array of small-aperture mirrors. In addition to eliminating the need for a large optic, the surface



An Array of Small Flat Mirrors would be used in a self-referencing, double-pass version of the Hartmann test configuration.

figure requirement for the small mirrors is relaxed compared to that required of the large autocollimation flat. The key point that allows this method to work is that the small mirrors need to operate as a monolithic flat only with regard to tip/tilt and not piston because in collimated space piston has no effect on the image centroids. The problem of aligning the small mirrors in tip/tilt requires a two-part solution. First, each mirror is suspended from a two-axis gimbal. The orientation of the gimbal is maintained by gravity. Second, the mirror is aligned such that the mirror normal is parallel to gravity vector. This is accomplished interferometrically in a test fixture. Of course, the test fixture itself needs to be calibrated with respect to gravity.

Another significant advantage of the array of gimballed small mirrors is the tolerance of the apparatus to thermal and mechanical perturbations. The individual mirrors are not affected by thermal distortions of the array structure because their orientation is self-correcting. That is, the pointing is maintained by gravity, not their supporting structure. Likewise, vibrations will cause the mirrors to sway about their equilibrium position. Thus, integrating the pencil beam image centroids over a sufficiently long period of time will make the measurements insensitive to vibration.

*This work was done by Robert P. Korechoff and Jeffrey M. Oseas of Caltech for NASA's Jet Propulsion Laboratory. Further information is contained in a TSP (see page 1). NPO-46118*

# Measuring a Fiber-Optic Delay Line Using a Mode-Locked Laser

Fractional error is no more than about  $3 \times 10^{-6}$ .

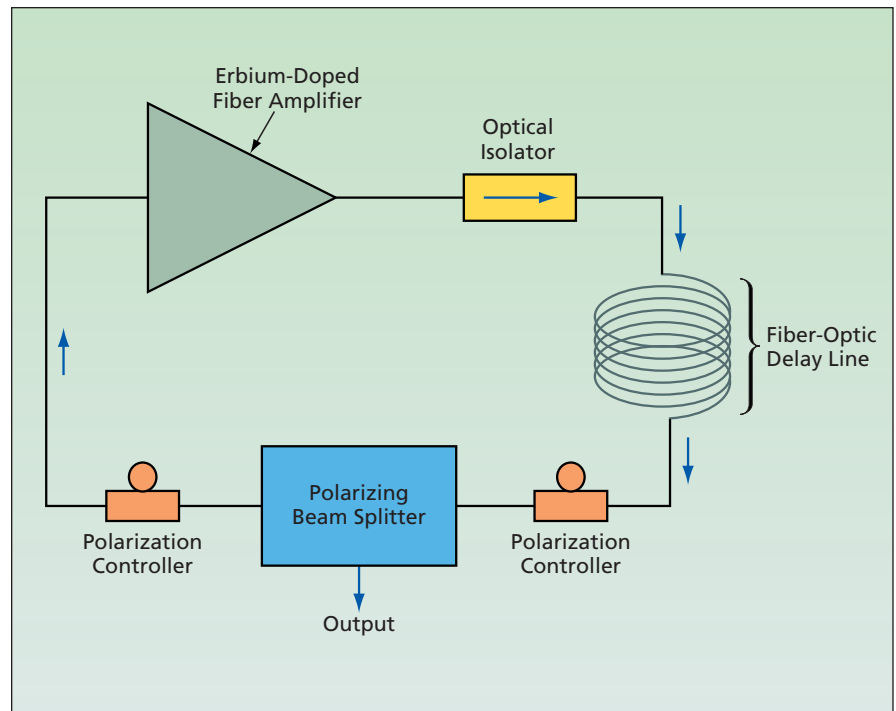
NASA's Jet Propulsion Laboratory, Pasadena, California

The figure schematically depicts a laboratory setup for determining the optical length of a fiber-optic delay line at a precision greater than that obtainable by use of optical time-domain reflectometry or of mechanical measurement of length during the delay-line-winding process. In this setup, the delay line becomes part of the resonant optical cavity that governs the frequency of oscillation of a mode-locked laser. The length can then be determined from frequency-domain measurements, as described below.

The laboratory setup is basically an all-fiber ring laser in which the delay line constitutes part of the ring. Another part of the ring — the laser gain medium — is an erbium-doped fiber amplifier pumped by a diode laser at a wavelength of 980 nm. The loop also includes an optical isolator, two polarization controllers, and a polarizing beam splitter. The optical isolator enforces unidirectional lasing. The polarizing beam splitter allows light in only one polarization mode to pass through the ring; light in the orthogonal polarization mode is rejected from the ring and utilized as a diagnostic output, which is fed to an optical spectrum analyzer and a photodetector. The photodetector output is fed to a radio-frequency spectrum analyzer and an oscilloscope. The fiber ring laser can generate continuous-wave radiation in non-mode-locked operation or ultra-short optical pulses in mode-locked operation.

The mode-locked operation exhibited by this ring is said to be passive in the sense that no electro-optical modulator or other active optical component is used to achieve it. Passive mode locking is achieved by exploiting optical nonlinearity of passive components in such a manner as to obtain ultra-short optical pulses. In this setup, the particular nonlinear optical property exploited to achieve passive mode locking is nonlinear polarization rotation.

This or any ring laser can support oscillation in multiple modes as long as sufficient gain is present to overcome losses in the ring. When mode locking is achieved, oscillation occurs in all the



An All-Fiber Ring Laser is configured alternately with and without the fiber-optic delay line as part of the ring. The length of the fiber-optic delay line is calculated from the FSRs of the laser in mode-locked operation in the two configurations.

modes having the same phase and same polarization. The frequency interval between modes, often denoted the free spectral range (FSR), is given by  $c/nL$ , where  $c$  is the speed of light in vacuum,  $n$  is the effective index of refraction of the fiber, and  $L$  is the total length of optical path around the ring. Therefore, the length of the fiber-optic delay line, as part of the length around the ring, can be calculated from the FSRs measured with and without the delay line incorporated into the ring. For this purpose, the FSR measurements are made by use of the optical and radio-frequency spectrum analyzers.

In experimentation on a 10-km-long fiber-optic delay line, it was found that this setup made it possible to measure the length to within a fractional error of about  $3 \times 10^{-6}$ , corresponding to a length error of 3 cm. In contrast, measurements by optical time-domain reflectometry and mechanical measurement were found to be much less

precise: For optical time-domain reflectometry, the fractional error was found no less than  $10^{-4}$  (corresponding to a length error of 1 m) and for mechanical measurement, the fractional error was found to be about  $10^{-2}$  (corresponding to a length error of 100 m).

*This work was done by Meirong Tu, Michael R. McKee, Kyung S. Pak, and Nan Yu of Caltech for NASA's Jet Propulsion Laboratory.*

*In accordance with Public Law 96-517, the contractor has elected to retain title to this invention. Inquiries concerning rights for its commercial use should be addressed to:*

*Innovative Technology Assets Management  
JPL*

*Mail Stop 202-233  
4800 Oak Grove Drive  
Pasadena, CA 91109-8099*

*E-mail: iaoffice@jpl.nasa.gov*

*Refer to NPO-45891, volume and number of this NASA Tech Briefs issue, and the page number.*



## Reconfigurable Hardware for Compressing Hyperspectral Image Data

Multiple hardware cores can be combined to increase throughput.

NASA's Jet Propulsion Laboratory, Pasadena, California

High-speed, low-power, reconfigurable electronic hardware has been developed to implement ICER-3D, an algorithm for compressing hyperspectral-image data. The algorithm and parts thereof have been the topics of several *NASA Tech Briefs* articles, including "Context Modeler for Wavelet Compression of Hyperspectral Images" (NPO-43239) and "ICER-3D Hyperspectral Image Compression Software" (NPO-43238), which appear elsewhere in this issue of *NASA Tech Briefs*. As described in more detail in those articles, the algorithm includes three main subalgorithms: one for computing wavelet transforms, one for context modeling, and one for entropy encoding. For the purpose of designing the hardware, these subalgorithms are treated as modules to be implemented efficiently in field-programmable gate arrays (FPGAs).

The design takes advantage of industry-standard, commercially available FPGAs. The implementation targets the Xilinx Virtex II pro architecture, which has embedded PowerPC processor cores with flexible on-chip bus architecture. It incorporates an efficient parallel and pipelined architecture to compress the three-dimensional image data. The design provides for internal buffering to minimize intensive input/output operations while making efficient use of off-chip memory. The design is scalable in that the subalgorithms are implemented as independent hardware modules that can be combined in parallel to increase throughput. The on-chip processor manages the overall operation of the compression system, including execution of the top-level control functions as well as scheduling, initiating, and monitoring processes.

The design prototype has been demonstrated to be capable of compressing hyperspectral data at a rate of 4.5 megasamples per second at a conservative clock frequency of 50 MHz, with a potential for substantially greater throughput at a higher clock frequency. The power consumption of the prototype is less than 6.5 W.

The reconfigurability (by means of reprogramming) of the FPGAs makes it possible to effectively alter the design to some extent to satisfy different requirements without adding hardware. The implementation could be easily propagated to future FPGA generations and/or to custom application-specific integrated circuits.

*This work was done by Nazeeh Aranki, Jeffrey Namkung, Carlos Villalpando, Aaron Kiely, Matthew Klimesh, and Hua Xie of Caltech for NASA's Jet Propulsion Laboratory. Further information is contained in a TSP (see page 1). NPO-42834*

## Spatio-Temporal Equalizer for a Receiving-Antenna Feed Array

Suppression of multipath effects and robust pointing would be achieved.

NASA's Jet Propulsion Laboratory, Pasadena, California

A spatio-temporal equalizer has been conceived as an improved means of suppressing multipath effects in the reception of aeronautical telemetry signals, and may be adaptable to radar and aeronautical communication applications as well. This equalizer would be an integral part of a system that would also include a seven-element planar array of receiving feed horns centered at the focal point of a paraboloidal antenna that would be nominally aimed at or near the aircraft that would be the source of the signal that one seeks to receive (see Figure 1). This spatio-temporal equalizer would consist mostly of a bank of seven adaptive finite-impulse-response (FIR) filters — one

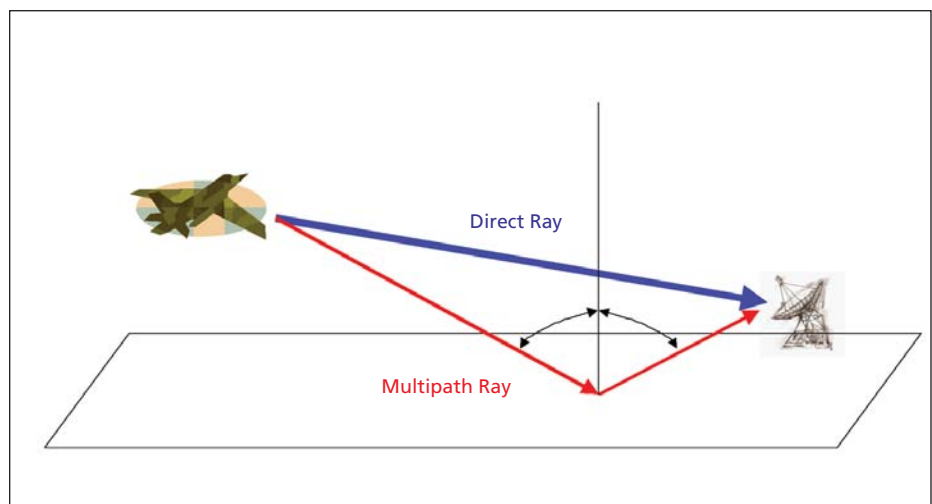


Figure 1. Signals Received by a Focal-Plane Array of feed horns would be processed by the spatio-temporal equalizer to suppress multipath effects and extract antenna-pointing information.

for each element in the array — and the outputs of the filters would be summed (see Figure 2). The combination of the spatial diversity of the feed-horn array and the temporal diversity of the filter bank would afford better multipath-suppression performance than is achievable by means of temporal equalization alone.

The seven-element feed array would supplant the single feed horn used in a conventional paraboloidal ground telemetry-receiving antenna. The radio-frequency telemetry signals received by the seven elements of the array would be digitized, converted to complex baseband form, and sent to the FIR filter bank, which would adapt itself in real time to enable reception of telemetry at a low bit error rate, even in the presence of multipath of the type found at many flight test ranges.

Each channel (comprising the signal-processing chain for a receiving feed horn) would contain an  $N$ -stage FIR filter. The incoming complex baseband signal in the  $i$ th channel at the  $n$ th sampling instant is denoted by  $y_i(n)$ . A filter weight at that instant is denoted generally by  $w_{i,j}(n)$ , where  $i$  is the index number of the channel ( $1 \leq i \leq 7$ ) and  $j$  is the index number of the filter stage ( $0 \leq j \leq N - 1$ ). The signal-combining operation at the summation (output) point of the FIR filter bank is given by

$$z(n) = \sum_{i=1}^7 \sum_{j=0}^{N-1} w_{i,j}^*(n) y_i(n-j),$$

where  $w_{i,0} \equiv 1$ . The weights would be adapted by an algorithm known in the

art as the constant-modulus algorithm, embodied in the following equation:

$$w_{i,j}(n+1) = w_{i,j}(n) + \alpha y_i(n-j) z^*(n) [1 - |z(n)|^2],$$

where  $\alpha$  is an adaptation rate parameter.

In addition, the combination of the array and the filter bank would make it

tion would be indicative of the difference between the antenna pointing direction and the actual directions of the direct and reflected beams, would be contained in the adaptive FIR weights. This information would be fed to a pointing estimator, which would generate instantaneous estimates of the difference between the antenna-pointing and target directions. The time series of these estimates would be sent to a set of Kalman filters, which would perform smoothing and prediction of the time series and extract velocity and acceleration estimates from the time series. The outputs of the Kalman filters would be sent to a unit that would control the pointing of the antenna, enabling robust pointing even in the presence of multipath.

The performances of several receiving systems with and without multipath and both with and without several conceptual versions of the spatio-temporal equalizer have been demonstrated in computational simulations. It was planned to begin construction of a breadboard version of the spatio-temporal equalizer at or about the time of writing this article.

This work was done by Ryan Mukai, Dennis Lee, and Victor Vilnrotter of Caltech for NASA's Jet Propulsion Laboratory. Further information is contained in a TSP (see page 1). This invention is owned by NASA, and a patent application has been filed. Inquiries concerning nonexclusive or exclusive license for its commercial development should be addressed to the Patent Counsel, NASA Management Office-JPL. Refer to NPO-43077.

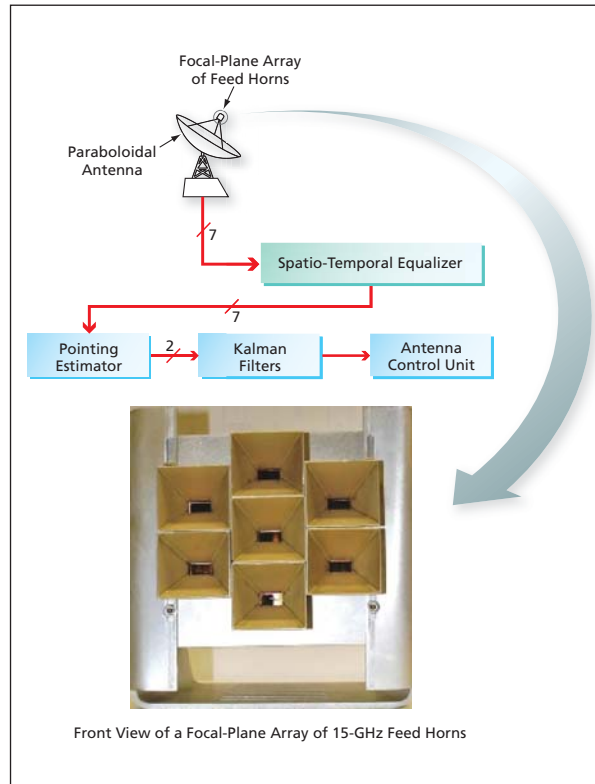


Figure 2. Seven FIR Filters would process the seven incoming signals, and the outputs of the filters would be summed.

possible to extract, in real time, pointing information that could be used to identify both the main beam traveling directly from the target aircraft and the beam that reaches the antenna after reflection from the ground: Information on the relative amplitudes and phases of the incoming signals, which informa-

## High-Speed Ring Bus

The ring bus is an enhancement of the general high-speed spacecraft bus.

NASA's Jet Propulsion Laboratory, Pasadena, California

The high-speed ring bus at the Jet Propulsion Laboratory (JPL) allows for future growth trends in spacecraft seen with future scientific missions. This innovation constitutes an enhancement of the 1393 bus as documented in the Institute of Electrical and Electronics Engineers (IEEE) 1393-1999 standard for a spaceborne fiber-optic data bus. It allows

for high-bandwidth and time synchronization of all nodes on the ring. The JPL ring bus allows for interconnection of active units with autonomous operation and increased fault handling at high bandwidths. It minimizes the flight software interface with an intelligent physical layer design that has few states to manage as well as simplified testability.

The design will soon be documented in the AS-1393 standard (Serial Hi-Rel Ring Network for Aerospace Applications).

The framework is designed for "Class A" spacecraft operation and provides redundant data paths. It is based on "fault containment regions" and "redundant functional regions (RFR)" and has a method for allocating cables that com-

pletely supports the redundancy in spacecraft design, allowing for a complete RFR to fail. This design reduces the mass of the bus by incorporating both the Control Unit and the Data Unit in the same hardware.

The standard uses ATM (asynchronous transfer mode) packets, standardized by ITU-T, ANSI, ETSI, and the ATM Forum. The IEEE-1393 standard uses the UNI form of the packet and provides no protection for the data portion of the cell. The JPL design adds optional formatting to this data portion. This design extends fault protection beyond that of the interconnect. This includes adding protection to the data portion that is contained within the Bus Interface Units (BIUs) and by adding to the signal interface between the Data Host and the JPL 1393 Ring Bus. Data

transfer on the ring bus does not involve a master or initiator. Following bus protocol, any BIU may transmit data on the ring whenever it has data received from its host. There is no centralized arbitration or bus granting.

The JPL design provides for autonomous synchronization of the nodes on the ring bus. An address-synchronous latency adjust buffer (LAB) has been designed that cannot get out of synchronization and needs no external input. Also, a priority-driven cable selection behavior has been programmed into each unit on the ring bus. This makes the bus able to connect itself up, according to a maximum redundancy priority system, without the need for computer intervention at startup. Switching around a failed or switched-off unit is also autonomous. The JPL bus provides a map of all the ac-

tive units for the host computer to read and use for fault management.

With regard to timing, this enhanced bus recognizes coordinated timing on a spacecraft as critical and addresses this with a single source of absolute and relative time, which is broadcast to all units on the bus with synchronization maintained to the tens of nanoseconds. Each BIU consists of up to five programmable triggers, which may be programmed for synchronization of events within the spacecraft of instrument. All JPL-formatted data transmitted on the ring bus are automatically time-stamped.

*This work was done by Terry Wysocky; Edward Kopf, Jr.; Sunant Katanyoutanant; Carl Steiner; and Harry Balian of Caltech for NASA's Jet Propulsion Laboratory. Further information is contained in a TSP (see page 1). NPO-42112*

## Nanoionics-Based Switches for Radio-Frequency Applications

These switches might supplant semiconductor and MEMS switches in some applications.

John H. Glenn Research Center, Cleveland, Ohio

Nanoionics-based devices have shown promise as alternatives to microelectromechanical systems (MEMS) and semiconductor diode devices for switching radio-frequency (RF) signals in diverse systems. Examples of systems that utilize RF switches include phase shifters for electronically steerable phased-array antennas, multiplexers, cellular telephones and other radio transceivers, and other portable electronic devices.

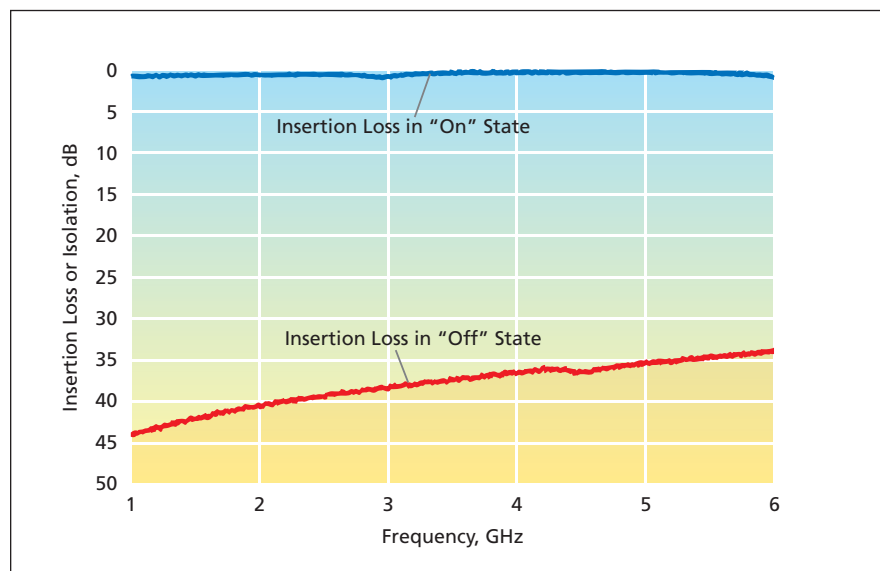
Semiconductor diode switches can operate at low potentials (about 1 to 3 V) and high speeds (switching times of the order of nanoseconds) but are characterized by significant insertion loss, high DC power consumption, low isolation, and generation of third-order harmonics and intermodulation distortion (IMD). MEMS-based switches feature low insertion loss (of the order of 0.2 dB), low DC power consumption (picowatts), high isolation (>30 dB), and low IMD, but contain moving parts, are not highly reliable, and must be operated at high actuation potentials (20 to 60 V) generated and applied by use of complex circuitry. In addition, fabrication of MEMS is complex, involving many processing steps.

Nanoionics-based switches offer the superior RF performance and low power consumption of MEMS switches, without need for the high potentials

and complex circuitry necessary for operation of MEMS switches. At the same time, nanoionics-based switches offer the high switching speed of semiconductor devices. Also, like semiconductor devices, nanoionics-based switches can be fabricated relatively inexpensively by use of conventional integrated-circuit fabrication techniques. Moreover, nanoionics-based switches have simple planar structures that can easily be inte-

grated into RF power-distribution circuits.

Nanoionics-based switches exploit the properties of some amorphous materials (in particular, chalcogenide glasses) that can incorporate relatively large amounts of metal and behave as solid electrolytes. The ionic conductivity of such a material can be of the same order of magnitude as the electronic conductivity of a semiconductor. Under appropriate bias con-



**Insertion Loss and Isolation** — two key switch characteristics — were measured in a test of a nanoionics-based switch over the frequency range of 1 to 6 GHz. The switch characteristics plotted here are comparable and/or superior to those of MEMS and semiconductor switches.

ditions (typically between 1 and 3 V), ions of a metal (silver) are formed at an anode made of that metal and migrate into the solid electrolyte while electrons (typically at a current of the order of microamperes to milliamperes) are injected from an electrochemically inert (nickel) cathode into the solid electrolyte. The injected electrons reduce the metal anions in the solid electrolyte, thereby causing the growth of metal nanowires through the electrolyte from the cathode to the corresponding anode.

Once a nanowire has grown sufficiently to form an electrically conductive path between the electrodes, there is no need to continue to apply electric power to maintain the connection. The process of making the connection can be easily reversed by applying a reverse bias to re-

oxidize the metal atoms in the solid electrolyte to recreate the insulating amorphous layer. Thus, a nanoionics-based switch is a reversible electrochemical switch that can have geometric features as small as nanometers. The process time for making or breaking the connection is about a nanosecond.

Experimental nanoionics based-switches having several different configurations have been built and tested in a continuing effort to gain understanding of the underlying chemical and physical principles and optimize designs. Fabrication of each experimental switch began with deposition of a binary chalcogenide glass on a high-resistivity silicon wafer. Next, a layer of silver was deposited on the glass and exposed to ultraviolet light to induce a photodissolution process in which silver ions mi-

grated into the glass matrix. Then an electrode of silver and an electrode of nickel were deposited on the chalcogenide layer.

The figure shows plots of data from a test of one of the experimental switches. Over the frequency range from 1 to 6 GHz, the insertion loss of the switch in the “on” state was less than 0.5 dB, while the isolation in the “off” state exceeded 30 dB.

*This work was done by James Nessel and Richard Lee of Glenn Research Center. Further information is contained in a TSP (see page 1).*

*Inquiries concerning rights for the commercial use of this invention should be addressed to NASA Glenn Research Center, Innovative Partnerships Office, Attn: Steve Fedor, Mail Stop 4-8, 21000 Brookpark Road, Cleveland, Ohio 44135. Refer to LEW-18313-1.*

---

## Lunar Dust-Tolerant Electrical Connector

*John H. Glenn Research Center, Cleveland, Ohio*

An electrical connector was developed that is tolerant of the presence of lunar dust. Novel features of the connector include the use of a permeable membrane to act both as a dust barrier and as a wiper to limit the amount of dust that makes its way into the internal chamber of the connector. The development focused on the Constellation lunar extravehicular activity (EVA) spacesuit's portable life support system (PLSS) battery recharge connector; however, continued research is applying this technology to other lunar surface systems such as lunar rover subsystems and cryogenic fluid transfer connections for *in-situ* resource utilization (ISRU) applications.

Lunar dust has been identified as a significant and present challenge in fu-

ture exploration missions. In addition to posing contamination and health risks for human explorers, the interlocking, angular nature of lunar dust and its broad grain size distribution make it particularly harmful to mechanisms with which it may come into contact. All Apollo lunar missions experienced some degree of equipment failure because of dust, and it appears that dust accumulation on exposed material is unavoidable and difficult to reverse. Both human EVA and ISRU activities are on the mission horizon and are paramount to the establishment of a permanent human base on the Moon. Reusable and dust-tolerant connection mechanisms are a critical component for mission success.

The need for dust-tolerant solutions is also seen in utility work and repair, mass transit applications, construction, mining, arctic and marine environments, diving (search and rescue), and various operations in deserts, where dust or sand clogging and coating different mechanisms and connections may render them difficult to operate or entirely inoperable.

*This work was done by Jason Herman, Shazad Sadick, and Dustyn Roberts of Honeybee Robotics Spacecraft Mechanisms Corporation for Glenn Research Center.*

*Inquiries concerning rights for the commercial use of this invention should be addressed to NASA Glenn Research Center, Innovative Partnerships Office, Attn: Steve Fedor, Mail Stop 4-8, 21000 Brookpark Road, Cleveland, Ohio 44135. Refer to LEW-18400-1.*

---

## Compact, Reliable EEPROM Controller

**This controller prevents inadvertent writes in an EEPROM.**

*Goddard Space Flight Center, Greenbelt, Maryland*

A compact, reliable controller for an electrically erasable, programmable read-only memory (EEPROM) has been developed specifically for a space-flight application. The design may be adaptable to other applications in which there are requirements for reliability in general and, in particular, for preven-

tion of inadvertent writing of data in EEPROM cells.

Inadvertent writes pose risks of loss of reliability in the original space-flight application and could pose such risks in other applications. Prior EEPROM controllers are large and complex and do not provide all reasonable protec-

tions (in many cases, few or no protections) against inadvertent writes. In contrast, the present controller provides several layers of protection against inadvertent writes. The controller also incorporates a write-time monitor, enabling determination of trends in the performance of an EEP-

ROM through all phases of testing.

The controller has been designed as an integral subsystem of a system that includes not only the controller and the controlled EEPROM aboard a spacecraft but also computers in a ground control station, relatively simple onboard support circuitry, and an onboard communication subsystem that utilizes the MIL-STD-1553B protocol. (MIL-STD-1553B is a military standard that encompasses a method of communication and electrical-interface re-

quirements for digital electronic subsystems connected to a data bus. MIL-STD-1553B is commonly used in defense and space applications.) The intent was to both maximize reliability while minimizing the size and complexity of onboard circuitry.

In operation, control of the EEPROM is effected via the ground computers, the MIL-STD-1553B communication subsystem, and the onboard support circuitry, all of which, in combination, provide the multiple layers of protection

against inadvertent writes. There is no controller software, unlike in many prior EEPROM controllers; software can be a major contributor to unreliability, particularly in fault situations such as the loss of power or brownouts. Protection is also provided by a power-monitoring circuit.

*This work was done by Richard Katz and Igor Kleyner of Goddard Space Flight Center. For further information, contact the Goddard Innovative Partnerships Office at (301) 286-5810. GSC-15492-1*

---

## Quad-Chip Double-Balanced Frequency Tripler

**This technology has uses such as high-resolution radar and spectroscopic screening.**

*NASA's Jet Propulsion Laboratory, Pasadena, California*

Solid-state frequency multipliers are used to produce tunable broadband sources at millimeter and submillimeter wavelengths. The maximum power produced by a single chip is limited by the electrical breakdown of the semiconductor and by the thermal management properties of the chip. The solution is to split the drive power to a frequency tripler using waveguides to divide the power among four chips, then recombine the output power from the four chips back into a single waveguide.

To achieve this, a waveguide branch-line quadrature hybrid coupler splits a 100-GHz input signal into two paths with a 90° relative phase shift. These two paths are split again by a pair of waveguide Y-junctions. The signals from the

four outputs of the Y-junctions are tripled in frequency using balanced Schottky diode frequency triplers before being recombined with another pair of Y-junctions. A final waveguide branch-line quadrature hybrid coupler completes the combination.

Using four chips instead of one enables using four-times higher power input, and produces a nearly four-fold power output as compared to using a single chip. The phase shifts introduced by the quadrature hybrid couplers provide isolation for the input and output waveguides, effectively eliminating standing waves between it and surrounding components. This is accomplished without introducing the high losses and expense of ferrite isolators.

A practical use of this technology is to drive local oscillators as was demonstrated around 300 GHz for a heterodyne spectrometer operating in the 2–3-THz band. Heterodyne spectroscopy in this frequency band is especially valuable for astrophysics due to the presence of a very large number of molecular spectral lines. Besides high-resolution radar and spectrographic screening applications, this technology could also be useful for laboratory spectroscopy.

*This work was done by Robert H. Lin, John S. Ward, Peter J. Bruneau, and Imran Mehdi of Caltech; Bertrand C. Thomas of Oak Ridge Associated Universities; and Alain Maestrini of the Observatoire de Paris for NASA's Jet Propulsion Laboratory. Further information is contained in a TSP (see page 1). NPO-46567*

---

## Ka-Band Waveguide Two-Way Hybrid Combiner for MMIC Amplifiers

**This technology is applicable as a power combiner for solid-state power amplifiers (SSPAs) with unequal and arbitrary power output ratios.**

*John H. Glenn Research Center, Cleveland, Ohio*

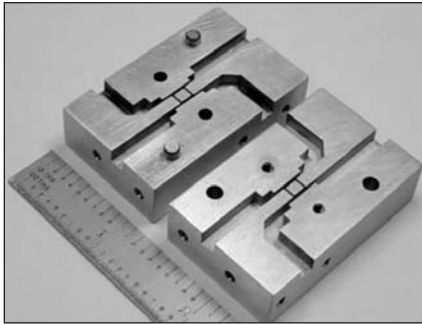
The design, simulation, and characterization of a novel Ka-band (32.05±0.25 GHz) rectangular waveguide two-way branch-line hybrid unequal power combiner (with port impedances matched to that of a standard WR-28 waveguide) has been created to combine input signals, which are in phase and with an amplitude ratio of two. The measured return loss and isolation of the branch-line hybrid are better than 22 and 27 dB, respectively. The

measured combining efficiency is 92.9 percent at the center frequency of 32.05 GHz. This circuit is efficacious in combining the unequal output power from two Ka-band GaAs pseudomorphic high electron mobility transistor (pHEMT) monolithic microwave integrated circuit (MMIC) power amplifiers (PAs) with high efficiency.

The component parts include the branch-line hybrid-based power combiner and the MMIC-based PAs. A two-

waybranch-line hybrid is a four-port device with all ports matched; power entering port 1 is divided in phase, and into the ratio 2:1 between ports 3 and 4. No power is coupled to port 2.

MMICs are a type of integrated circuit fabricated on GaAs that operates at microwave frequencies, and performs the function of signal amplification. The power combiner is designed to operate over the frequency band of 31.8 to 32.3



The fabricated **Two-Way Ka-Band Branch-Line Hybrid Unequal Power Combiner** in E-plane split block arrangement. The dimensions of the assembled combiner are 1.8×1.2×1 in. (=4.7×3.0×2.5 cm).

GHz, which is NASA's deep space frequency band. The power combiner would have an output return loss better than 20 dB. Isolation between the output port and the isolated port is greater than 25 dB. Isolation between the two input

ports is greater than 25 dB. The combining efficiency would be greater than 90 percent when the ratio of the two input power levels is two. The power combiner is machined from aluminum with E-plane split-block arrangement, and has excellent reliability.

The flexibility of this design allows the combiner to be customized for combining the power from MMIC PAs with an arbitrary power output ratio. In addition, it allows combining a low-power GaAs MMIC with a high-power GaN MMIC. The arbitrary port impedance allows matching the output impedance of the MMIC PA directly to the waveguide impedance without transitioning first into a transmission line with characteristic impedance of 50 ohms. Thus, by eliminating the losses associated with a transition, the overall SSPA efficiency is enhanced.

For reducing the cost and weight when required in very large quantities,

such as in the beam-forming networks of phased-array antenna systems, the combiner can be manufactured using metal-plated plastic. Two hybrid unequal power combiners can be cascaded to realize a non-binary combiner (for e.g., a three-way) and can be synergistically optimized for low VSWR (voltage standing wave ratio), low insertion loss, high isolation, and wide bandwidth using commercial off-the-shelf electromagnetic software design tools.

*This work was done by Rainee N. Simons, Christine T. Chevalier, Edwin G. Wintucky, and Jon C. Freeman of Glenn Research Center. Further information is contained in a TSP (see page 1).*

*Inquiries concerning rights for the commercial use of this invention should be addressed to NASA Glenn Research Center, Innovative Partnerships Office, Attn: Steve Fedor, Mail Stop 4-8, 21000 Brookpark Road, Cleveland, Ohio 44135. Refer to LEW 18473-1.*

## Radiation-Hardened Solid-State Drive

*NASA's Jet Propulsion Laboratory, Pasadena, California*

A method is provided for a radiation-hardened (rad-hard) solid-state drive for space mission memory applications by combining rad-hard and commercial off-the-shelf (COTS) non-volatile memories (NVMs) into a hybrid architecture. The architecture is controlled by a rad-hard ASIC (application specific integrated circuit) or a FPGA (field programmable gate array). Specific error handling and data management protocols are developed for use in a rad-hard environment. The rad-hard memories are smaller in

overall memory density, but are used to control and manage radiation-induced errors in the main, and much larger density, non-rad-hard COTS memory devices.

Small amounts of rad-hard memory are used as error buffers and temporary caches for radiation-induced errors in the large COTS memories. The rad-hard ASIC/FPGA implements a variety of error-handling protocols to manage these radiation-induced errors. The large COTS memory is triplicated for protection, and CRC-based counters are

calculated for sub-areas in each COTS NVM array. These counters are stored in the rad-hard non-volatile memory. Through monitoring, rewriting, regeneration, triplication, and long-term storage, radiation-induced errors in the large NV memory are managed. The rad-hard ASIC/FPGA also interfaces with the external computer buses.

*This work was done by Douglas J. Sheldon of Caltech for NASA's Jet Propulsion Laboratory. Further information is contained in a TSP (see page 1). NPO-46925*



## Use of Nanofibers to Strengthen Hydrogels of Silica, Other Oxides, and Aerogels

John H. Glenn Research Center, Cleveland, Ohio

Research has shown that including up to 5 percent w/w carbon nanofibers in a silica backbone of polymer cross-linked aerogels improves its strength, tripling compressive modulus and increasing tensile stress-at-break five-fold with no increase in density or decrease in porosity. In addition, the initial silica hydrogels, which are produced as a first step in manufacturing the aerogels, can be quite fragile and difficult

to handle before cross-linking. The addition of the carbon nanofiber also improves the strength of the initial hydrogels before cross-linking, improving the manufacturing process. This can also be extended to other oxide aerogels, such as alumina or aluminosilicates, and other nanofiber types, such as silicon carbide.

*This work was done by Mary Ann B. Meador, Lynn A. Capadona, Frances Hur-*

*witz, and Stephanie L. Vivot of Glenn Research Center and Max Lake of Applied Sciences, Inc. Further information is contained in a TSP (see page 1).*

*Inquiries concerning rights for the commercial use of this invention should be addressed to NASA Glenn Research Center, Innovative Partnerships Office, Attn: Steve Fedor, Mail Stop 4-8, 21000 Brookpark Road, Cleveland, Ohio 44135. Refer to LEW-18380-1.*

## Two Concepts for Deployable Trusses

**Thermal-actuation and misalignment-tolerant double-pivot designs are proposed.**

Lyndon B. Johnson Space Center, Houston, Texas

Two concepts that could be applied separately or together have been suggested to enhance the utility of deployable truss structures. The concepts were intended originally for application to a truss structure to be folded for compact stowage during transport and subsequently deployed in outer space. The concepts may also be applicable, with some limitations, to deployable truss structures designed to be used on Earth.

The first concept involves a combination of features that would help to maximize reliability of a structure while minimizing its overall mass, the complexity of its deployment system, and the expenditure of energy for deployment. The deployment system would be integrated into the truss: some of the truss members would contain folding/unfolding-detent mechanisms similar to those in umbrellas; other truss members would contain shape-memory-alloy (SMA) coil actuators (see Figure 1). Upon exposure to sunlight, the SMA actuators would be heated above their transition temperature, causing them to extend to their deployment lengths. The extension of the actuators would cause the structure to unfold and, upon completion of un-

folding, the umbrellalike mechanisms would lock the unfolded truss in the fully deployed configuration. The use of solar heating to drive deployment would eliminate the need to carry a deployment power source. The actuation scheme would offer high reliability in that the truss geometry would be such that deployment could be completed even if all actuators were not function-

ing. Of course, in designing for operation in normal Earth gravitation, it would be necessary to ensure that the SMA actuators could apply forces large enough to overcome the deployment-resisting forces attributable to the weights of the members.

The second concept is that of an improved design for the joints in folding members. Before describing this design,

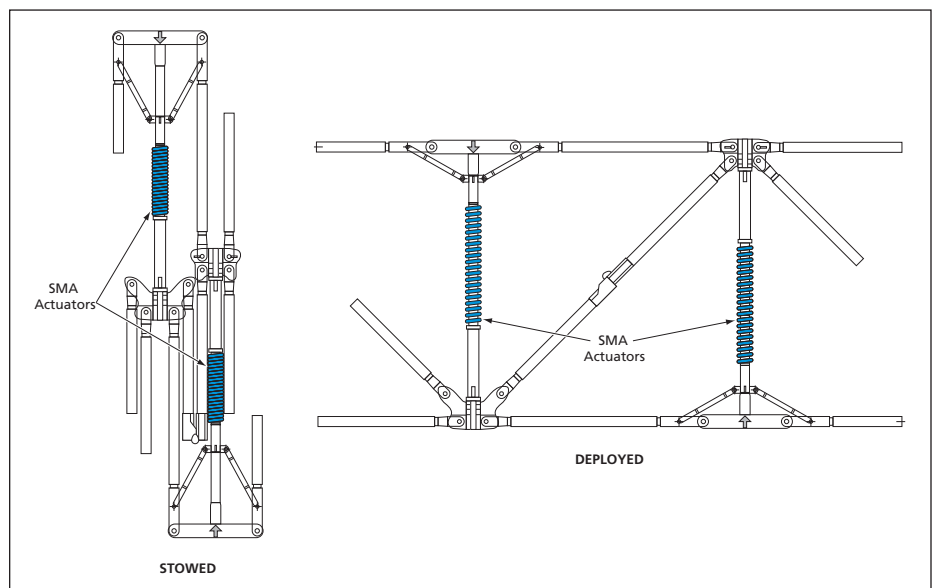


Figure 1. SMA Coil Actuators would apply forces to displace jointed members to unfold a truss structure from compact stowage to a fully deployed condition.

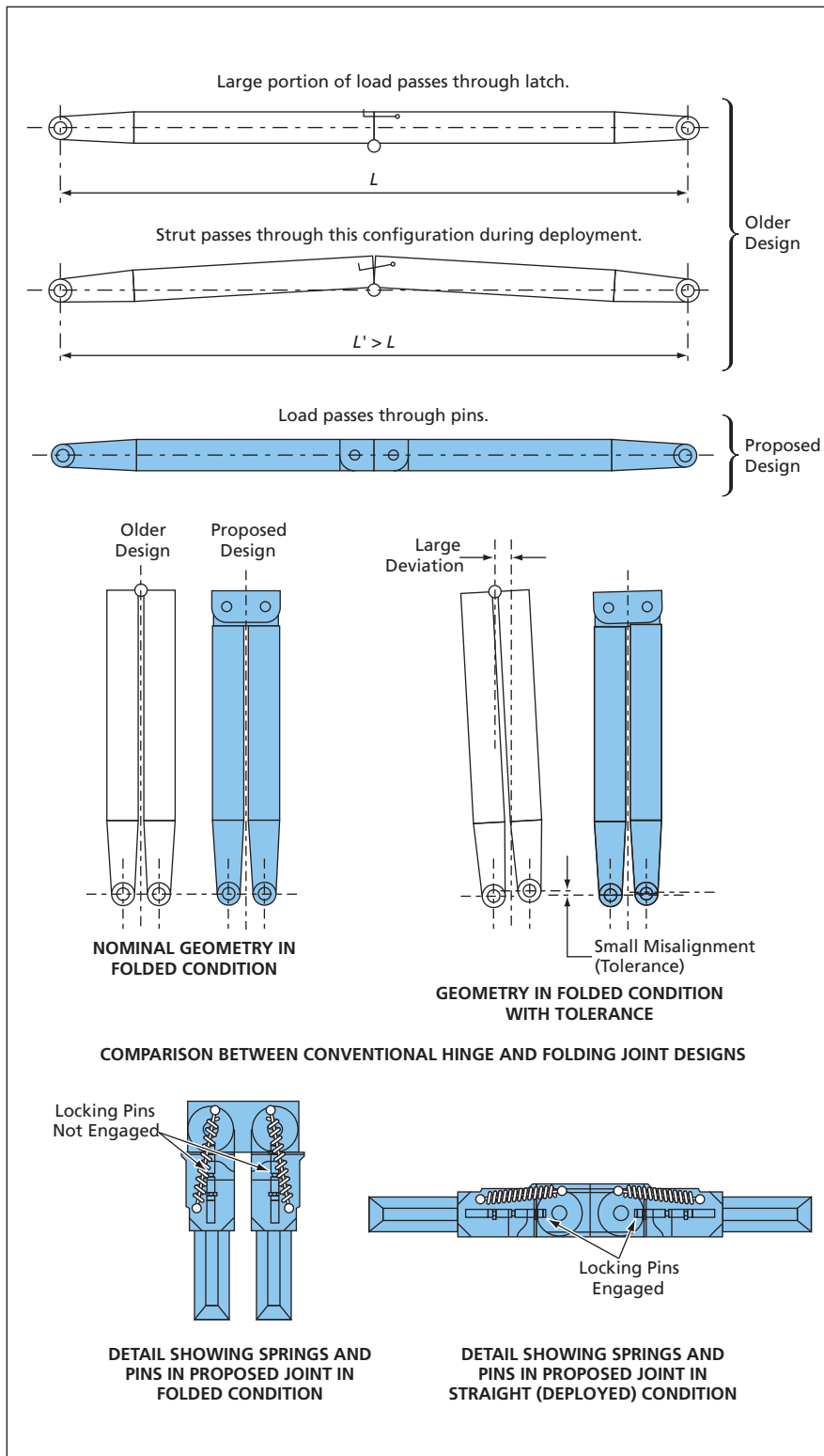


Figure 2. A **Proposed Double-Pivot Joint Design** would offer advantages over an older single-off-center-pivot design.

it is necessary to describe pertinent aspects of a prior design concept that this design concept is intended to supplant. In a typical folding truss structure of prior design, a joint in a folding member includes a pivot located away from the centerline on one side and a latch located away from the centerline on the opposite side (see Figure 2). This entails three disadvantages:

- Much of the load is borne by the latch. If the latch is spring-loaded, then the spring must be designed so that it poses only minimal resistance to unfolding and yet applies a substantial latching preload. At best, it is difficult to satisfy this combination of requirements, and the joint is vulnerable to dislocation during loading.
- The use of only one pivot necessitates adherence to tight tolerances in order to accommodate folding.
- Pivoting about an off-center point necessitates passage of the member through an “over-the-center” condition that may be undesirable.

The present second design concept calls for two pivots, located a short distance apart and nominally located on the centerline when the member is unfolded. In comparison with the single-off-center-pivot arrangement, the two-pivot arrangement could accommodate large misalignment in the folded condition. The joint would include two springs in an “over-the-center” configuration in which they would not apply deployment force while the member remained completely folded but would apply straightening force and torque during the final stages of deployment. Spring-loaded axial latching pins would snap into place at completion of deployment. Thereafter, the two pivots would bear the main axial load, while the latching pins would stabilize the joint against buckling.

*This work was done by John W. Renfro of The Boeing Company for Johnson Space Center. For further information, contact the JSC Innovation Partnerships Office at (281) 483-3809.*

*This invention is owned by NASA, and a patent application has been filed. Inquiries concerning nonexclusive or exclusive license for its commercial development should be addressed to the Patent Counsel, Johnson Space Center, (281) 483-1003. Refer to MSC-23848-1/4142-1.*



## Concentric Nested Toroidal Inflatable Structures

Interior volume can be partitioned more flexibly than in single larger structures.

Lyndon B. Johnson Space Center, Houston, Texas

Assemblies comprising multiple limited-height toroidal inflatable structures nested in a concentric arrangement have been invented to obtain more design flexibility than can be obtained in single taller, wider toroidal inflatable structures (see figure). Originally intended for use as containers for habitats for humans in outer space or on remote planets, these and related prior inflatable structures could also be useful on Earth as lightweight, compactly stowable, portable special-purpose buildings that could be transported to remote locations and there inflated to full size and shape.

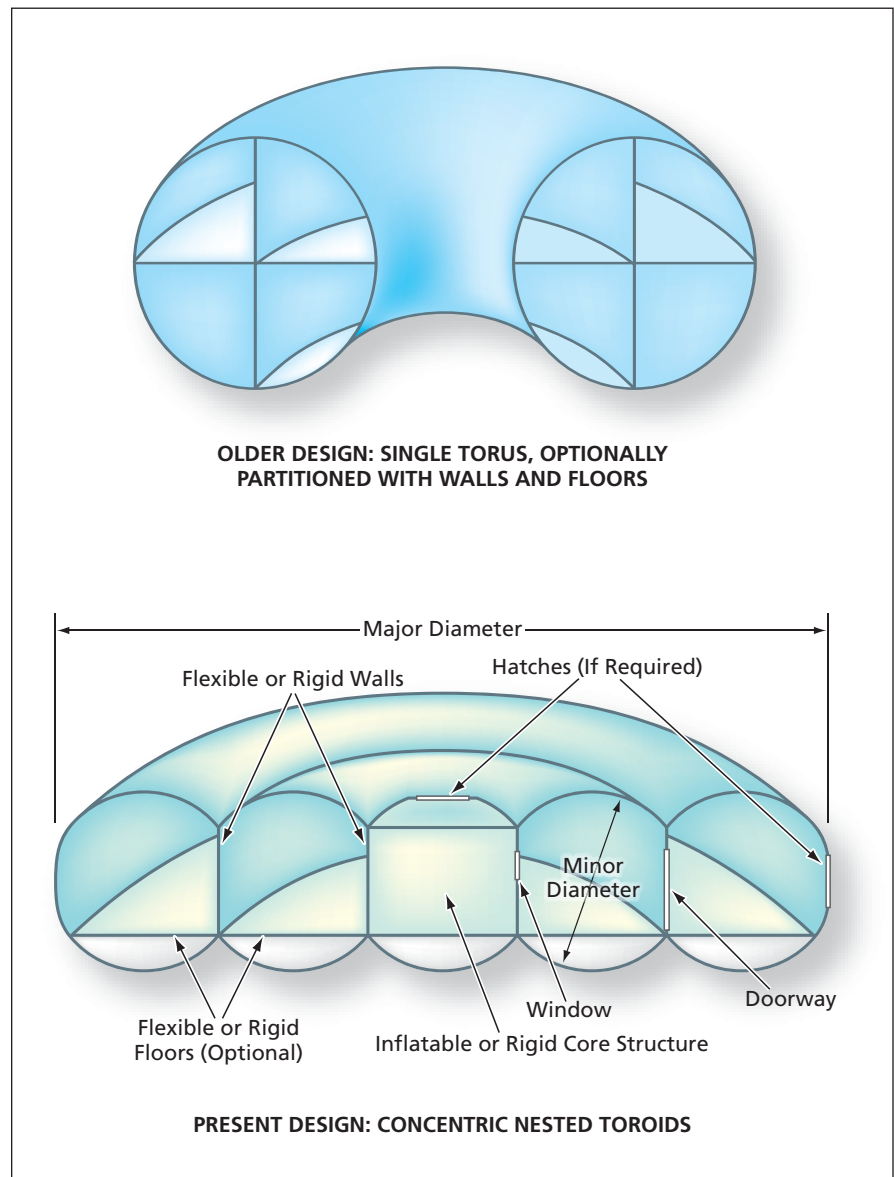
In the case of a single inflatable toroidal structure, one important source of lack of design flexibility is the fact that an increase in outer diameter (which is sometimes desired) is necessarily accompanied by an increase in height (which is sometimes undesired). Increases in diameter and height can also cause difficulty in utilization of the resulting larger volume, in that it can become necessary to partition the volume by means of walls and floors, and features (e.g., stairs or ladders) must be added to enable vertical movement between floors. Moreover, ascending and descending between floors in a gravitational environment could pose unacceptable difficulty for the inhabitants under some circumstances.

Another source of lack of design flexibility in a single toroidal inflatable structure is that for a given inflation pressure, an increase in the outer diameter of the structure necessarily entails an increase in the maximum stress in the structure. Because it is necessary to keep the maximum stress within the load-bearing capability of the structural materials, consistent with other aspects of the design, this may translate to a limit on the outer diameter.

In an assembly comprising concentric nested toroidal structures, an increase in outer diameter does not necessarily entail an increase in height or a maximum stress in excess of the load-bearing capa-

bility of the structural materials. The minor diameters of the nested toroid can be chosen to partition interior spaces optimally, without necessitating the addition of walls or floors. Inasmuch as the maximum stress in a nested inflatable toroidal structure is a function of its minor diameter and the minor diameter is typically small enough that the load-

bearing capability of the structural materials is not exceeded, there is no longer a limit on the outer diameter of the assembly: instead, the assembly can be expanded, without limit, by simply adding concentric inflatable toroidal structures having suitable minor diameters and successively larger major diameters. The minor diameters need not be equal: The



An Assembly of Concentric Toroidal Inflatable Structures offers advantages over a single taller, wider toroidal inflatable structure.

diameter of each concentric inflatable toroidal structure can be chosen according to the specific purpose(s) to be served by that structure.

Adjacent concentric inflatable toroidal structures can be separated by a flexible or rigid wall that bears the vertical (axial) load between the bottom and the top to prevent undesired axial expansion and thereby to help to maintain the desired overall shape of the assembly. The walls can incorporate penetra-

tions, including windows and hatches. In an extreme case, a wall can be removed if it is replaced with rigid bars that are (1) attached to the tops and the bottoms of the adjacent toroid and (2) connected together with circumferential tension-bearing members. Rigid or flexible floors can be integrated into the inflated toroidal structures. Preferably, the floors in adjacent toroids should be joined to the wall between the toroids at the same level.

*This work was done by Christopher J. Johnson, Jasen L. Raboin, and Gary R. Spexarth of Johnson Space Center. Further information is contained in a TSP (see page 1).*

*This invention is owned by NASA, and a patent application has been filed. Inquiries concerning nonexclusive or exclusive license for its commercial development should be addressed to the Patent Counsel, Johnson Space Center, (281) 483-0837. Refer to MSC-24215-1.*

## Investigating Dynamics of Eccentricity in Turbomachines

**Rotordynamic and hydrodynamic forces are measured under prescribed rotor-whirl conditions.**

*Marshall Space Flight Center, Alabama*

A methodology (and hardware and software to implement the methodology) has been developed as a means of investigating coupling between certain rotordynamic and hydrodynamic phenomena in turbomachines. Originally, the methodology was intended for application in an investigation of coupled rotordynamic and hydrodynamic effects postulated to have caused high synchronous vibration in the space shuttle's high-pressure oxygen turbopump (HPOTP). The methodology can also be applied in investigating (for the purpose of developing means of suppressing) undesired hydrodynamic rotor/stator interactions in turbomachines in general.

The methodology and the types of phenomena that can be investigated by use of the methodology are best summarized by citing the original application as an example. In that application, in consideration of the high synchro-

nous vibration in the space-shuttle main engine (SSME) HPOTP, it was determined to be necessary to perform tests to investigate the influence of inducer eccentricity and/or synchronous whirl motion on inducer hydrodynamic forces under prescribed flow and cavitation conditions. It was believed that manufacturing tolerances of the turbopump resulted in some induced runout of the pump rotor. Such runout, if oriented with an inducer blade, would cause that blade to run with tip clearance smaller than the tip clearances of the other inducer blades. It was hypothesized that the resulting hydraulic asymmetry, coupled with alternating blade cavitation, could give rise to the observed high synchronous vibration.

In tests performed to investigate this hypothesis, prescribed rotor whirl motions have been imposed on a 1/3-scale water-rig version of the SSME LPOTP

inducer (which is also a 4-bladed inducer having similar cavitation dynamics as the HPOTP) in a magnetic-bearing test facility. The particular magnetic-bearing test facility, through active vibration control, affords a capability to impose, on the rotor, whirl orbits having shapes and whirl rates prescribed by the user, and to simultaneously measure the resulting hydrodynamic forces generated by the impeller. Active control also made it possible to modulate the inducer-blade running tip clearance and consequently effect alternating blade cavitation. The measured hydraulic forces have been compared and correlated with shroud dynamic-pressure measurements.

*This work was done by Daniel Baun of Concepts NREC for Marshall Space Flight Center. For further information, contact Sammy Nabors, MSFC Commercialization Assistance Lead, at [sammy.a.nabors@nasa.gov](mailto:sammy.a.nabors@nasa.gov). Refer to MFS-32563-1.*



## Improved Low-Temperature Performance of Li-Ion Cells Using New Electrolytes

**This technology has utility in high-power batteries for electric vehicles.**

*NASA's Jet Propulsion Laboratory, Pasadena, California*

As part of the continuing efforts to develop advanced electrolytes to improve the performance of lithium-ion cells, especially at low temperatures, a number of electrolyte formulations have been developed that result in improved low-temperature performance (down to  $-60\text{ }^{\circ}\text{C}$ ) of 26650 A123Systems commercial lithium-ion cells. The cell type/design, in which the new technology has been demonstrated, has found wide application in the commercial sector (i.e., these cells are currently being used in commercial portable power tools). In addition, the technology is actively being considered for hybrid electric vehicle (HEV) and electric vehicle (EV) applications.

In current work, a number of low-temperature electrolytes have been developed based on advances involving lithium hexafluorophosphate-based solutions in carbonate and carbonate + ester solvent blends, which have been further optimized in the context of the technology and targeted applications. The approaches employed, which include the use of ternary mixtures of carbonates, the use of ester co-solvents

[e.g., methyl butyrate (MB)], and optimized lithium salt concentrations (e.g.,  $\text{LiPF}_6$ ), were compared with the commercial baseline electrolyte, as well as an electrolyte being actively considered for DoE HEV applications and previously developed by a commercial enterprise, namely  $\text{LiPF}_6$  in ethylene carbonate (EC) + ethyl methyl carbonate (EMC) (30:70%). The four new low-temperature electrolytes developed include:

1. 1.0 M  $\text{LiPF}_6$  EC+EMC+MB (30:40:30 v/v%),
2. 1.4 M  $\text{LiPF}_6$  EC+EMC+MB (30:40:30 v/v %),
3. 1.4 M  $\text{LiPF}_6$  EC+EMC+MB (10:10:80 v/v%), and
4. 1.0 M  $\text{LiPF}_6$  EC+DMC+EMC (30:20:50 v/v %).

Excellent high-discharge-rate performance was observed at  $-30$  and  $-40\text{ }^{\circ}\text{C}$  with cells containing these formulations, with up to 3.0C and 1.0C being capable, respectively, for most cells. For the 1.4 M  $\text{LiPF}_6$  EC+EMC+MB (10:10:80 v/v%) formulation, cells were observed to support 5.0C and 3.0C continuous discharge at  $-30$  and  $-40\text{ }^{\circ}\text{C}$ , respec-

tively, while charging the cells at low temperature. Good performance was obtained to temperatures as low as  $-60\text{ }^{\circ}\text{C}$  with over 57 W·h/kg being delivered at a C/20 rate. Cycling tests demonstrated that most cells had good life characteristics over a wide temperature range, with the all carbonate-based formulations being most robust. Given that some of the electrolytes described contain ester co-solvents, there is some concern that the systems will not perform well above ambient temperatures (i.e.,  $>40\text{ }^{\circ}\text{C}$ ). It is anticipated that improvement of the high-temperature stability of these systems can be achieved through the use of electrolyte additives, such as vinylene carbonate (VC), monofluoroethylene carbonate (FEC), dimethyl acetamide (DMAc), and/or the use of mixed salt solutions such as LiBOB and LiFAP used in conjunction with  $\text{LiPF}_6$ .

*This work was done by Marshall C. Smart and Ratnakumar V. Bugga of Caltech and Antoni S. Gozdz and Suresh Mani of A123Systems, Inc. for NASA's Jet Propulsion Laboratory. Further information is contained in a TSP (see page 1). NPO-46180*





## Integrity Monitoring of Mercury Discharge Lamps

NASA's Jet Propulsion Laboratory, Pasadena, California

Mercury discharge lamps are critical in many trapped ion frequency standard applications. An integrity monitoring system can be implemented using end-of-life signatures observed in operational mercury discharge lamps, making it possible to forecast imminent failure and to take action to mitigate the consequences (such as switching to a redundant system). Mercury lamps are used as a source of 194-nm ultraviolet radiation for optical pumping and state selection of mercury trapped ion frequency standards. Lamps are typically fabricated using  $^{202}\text{Hg}$  distilled into high-purity quartz, or other 194-nm transmitting material (e.g., sapphire). A buffer gas is also placed into the bulb, typically a noble gas such as argon, neon, or krypton.

The bulbs are driven by strong RF fields oscillating at  $\approx 200$  MHz. The lamp output may age over time by two internal mechanisms: (1) the darkening of the bulb that attenuates light transmission and (2) the loss of mercury due to migration or chemical interactions with the bulb surface. During fabrication, excess mercury is placed into a bulb, so that the loss rate is compensated with new mercury emanating from a cool tip or adjacent reservoir. The light output is nearly constant or varies slightly at a constant rate for many months/years until the mercury source is depleted. At this point, the vapor pressure abruptly falls and the total light output and atomic clock SNR (signal-to-noise ratio) decrease. After several days to weeks, the light levels decrease to a point

where the atomic clock SNR is no longer sufficient to stay in lock, or the lamp self-extinguishes.

This signature has been observed in four separate end-of-life lamp failures while operating in the Deep Space Network (DSN). A simple integrator circuit can observe and document steady-state lamp behavior. When the light levels drop over a predetermined time interval by a specified amount (e.g., 20 percent), an alarm is set. For critical operational applications, such as the DSN or in space flight, this warning provides notice that a failure may be imminent, and for operators or control algorithm to take action.

*This work was done by Robert L. Tjoelker of Caltech for NASA's Jet Propulsion Laboratory. For more information, contact iaof-[iaof@jpl.nasa.gov](mailto:iaof@jpl.nasa.gov). NPO-45650*

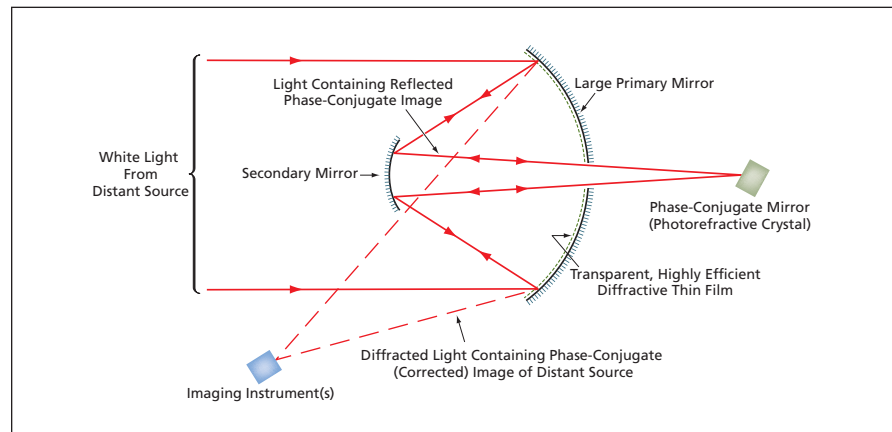
## White-Light Phase-Conjugate Mirrors as Distortion Correctors

Optical aberrations of large optical components could be corrected relatively inexpensively.

Marshall Space Flight Center, Alabama

White-light phase-conjugate mirrors would be incorporated into some optical systems, according to a proposal, as means of correcting for wavefront distortions caused by imperfections in large optical components. The proposal was given impetus by a recent demonstration that white, incoherent light can be made to undergo phase conjugation, whereas previously, only coherent light was known to undergo phase conjugation.

This proposal, which is potentially applicable to almost any optical system, was motivated by a need to correct optical aberrations of the primary mirror of the Hubble Space telescope. It is difficult to fabricate large optical components like the Hubble primary mirror and to ensure the high precision typically required of such components. In most cases, despite best efforts, the components as fabricated have small imperfections that introduce optical aberrations that adversely affect imaging quality.



A **Phase-Conjugate Mirror** would be added to a conventional primary-and-secondary-mirror telescope in the position ordinarily occupied by the imaging instrument(s). A transparent diffractive thin film would also be added to the primary mirror. The phase-conjugate (corrected) image would be diffracted onto the repositioned imaging instruments.

Correcting for such aberrations is difficult and costly. The proposed use of white-light phase conjugate mirrors offers a relatively simple and inexpensive solution of the aberration-correction

problem. Indeed, it should be possible to simplify the entire approach to making large optical components because there would be no need to fabricate those components with extremely high

precision in the first place: A white-light phase-conjugate mirror could correct for all the distortions and aberrations in an optical system. The use of white-light phase-conjugate mirrors would be essential for ensuring high performance in optical systems containing lightweight membrane mirrors, which are highly deformable.

As used here, “phase-conjugate mirror” signifies, more specifically, an optical component in which incident light undergoes time-reversal phase conjugation.

In practice, a phase-conjugate mirror would typically be implemented by use of a suitably positioned and oriented photorefractive crystal. In the case of a telescope comprising a primary and secondary mirror (see figure) white light from a distant source would not be brought to initial focus on one or more imaging scientific instrument(s) as in customary practice. Instead, the light would be brought to initial focus on a phase-conjugate mirror. The phase-conjugate mirror would send a phase-conju-

gate image back, along the path of the incoming light, to the primary mirror. A transparent, highly efficient diffractive thin film deposited on the primary mirror would direct the phase-conjugate image to the imaging instrument(s).

*This work was done by Donald Frazier and W. Scott Smith of Marshall Space Flight Center, Hossin Abdeldayem of Goddard Space Flight Center, and Partha Banerjee of the University of Dayton. For further information, contact Hossin Abdeldayem at [hossin.a.abdeldayem@nasa.gov](mailto:hossin.a.abdeldayem@nasa.gov). MFS-31683-1*

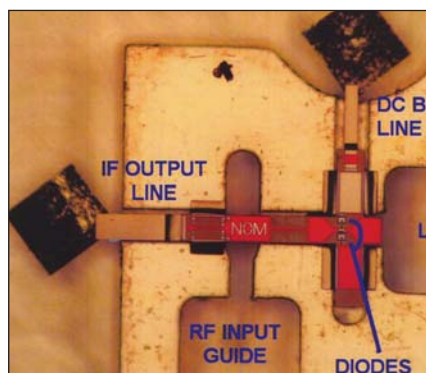
## Biasable, Balanced, Fundamental Submillimeter Monolithic Membrane Mixer

**Gallium arsenide membrane technology enables wide bandwidth and high operating frequencies.**

*NASA's Jet Propulsion Laboratory, Pasadena, California*

This device is a biasable, submillimeter-wave, balanced mixer fabricated using JPL's monolithic membrane process — a simplified version of planar membrane technology. The primary target application is instrumentation used for analysis of atmospheric constituents, pressure, temperature, winds, and other physical and chemical properties of the atmospheres of planets and comets. Other applications include high-sensitivity gas detection and analysis. This innovation uses a balanced configuration of two diodes allowing the radio frequency (RF) signal and local oscillator (LO) inputs to be separated. This removes the need for external diplexers that are inherently narrowband, bulky, and require mechanical tuning to change frequency. Additionally, this mixer uses DC bias-ability to improve its performance and versatility.

In order to solve problems relating to circuit size, the GaAs membrane process was created. As much of the circuitry as possible is fabricated on-chip, making the circuit monolithic. The remainder of the circuitry is precision-machined into a waveguide block that holds the GaAs circuit. The most critical alignments are performed using micron-scale semiconductor technology, enabling wide bandwidth and high operating fre-



In the **Balanced Mixer**, the diodes are at the right side of the circuit and the LO comes from the waveguide at the right into a reduced-height section containing the diodes. The RF signal is picked up from the RF waveguide by the probe on the left, and flows rightward to the diodes.

quencies. The balanced mixer gets superior performance with less than 2 mW of LO power. This can be provided by a simple two-stage multiplier chain following an amplifier at around 90 GHz. Further, the diodes are arranged so that they can be biased. Biasing pushes the diodes closer to their switching voltage, so that less LO power is required to switch the diodes on and off.

In the photo, the diodes are at the right end of the circuit. The LO comes

from the waveguide at the right into a reduced-height section containing the diodes. Because the diodes are in series to the LO signal, they are both turned on and off simultaneously once per LO cycle. Conversely, the RF signal is picked up from the RF waveguide by the probe at the left, and flows rightward to the diodes. Because the RF is in a quasi-TEM (suspended, microstrip-like) mode, it impinges on the diodes in an anti-parallel mode that does not couple to the waveguide mode. This isolates the LO and RF signals. This operation is similar to a cross-bar mixer used at low frequencies, except the RF signal enters through the back-short end of the waveguide rather than through the side. The RF probe also conveys the down-converted intermediate frequency (IF) signal out to an off-chip circuit board through a simple LC low-pass filter to the left as indicated. The bias is brought to the diodes through a bypass capacitor at the top.

*This work was done by Peter Siegel, Erich Schlecht, Imran Mehdi, John Gill, James Velebir, Raymond Tsang, Robert Dengler, and Robert Lin of Caltech for NASA's Jet Propulsion Laboratory. For more information, contact [iaoffice@jpl.nasa.gov](mailto:iaoffice@jpl.nasa.gov). NPO-44698*



## ICER-3D Hyperspectral Image Compression Software

Software has been developed to implement the ICER-3D algorithm. ICER-3D effects progressive, three-dimensional (3D), wavelet-based compression of hyperspectral images. If a compressed data stream is truncated, the progressive nature of the algorithm enables reconstruction of hyperspectral data at fidelity commensurate with the given data volume.

The ICER-3D software is capable of providing either lossless or lossy compression, and incorporates an error-containment scheme to limit the effects of data loss during transmission. The compression algorithm, which was derived from the ICER image compression algorithm, includes wavelet-transform, context-modeling, and entropy coding subalgorithms.

The 3D wavelet decomposition structure used by ICER-3D exploits correlations in all three dimensions of sets of hyperspectral image data, while facilitating elimination of spectral ringing artifacts, using a technique summarized in “Improving 3D Wavelet-Based Compression of Spectral Images” (NPO-41381), *NASA Tech Briefs*, Vol. 33, No. 3 (March 2009), page 7a.

Correlation is further exploited by a context-modeling subalgorithm, which exploits spectral dependencies in the wavelet-transformed hyperspectral data, using an algorithm that is summarized in “Context Modeler for Wavelet Compression of Hyperspectral Images” (NPO-43239), which follows this article.

An important feature of ICER-3D is a scheme for limiting the adverse effects of loss of data during transmission. In this scheme, as in the similar scheme used by ICER, the spatial-frequency domain is partitioned into rectangular error-containment regions. In ICER-3D, the partitions extend through all the wavelength bands. The data in each partition are compressed independently of those in the other partitions, so that loss or corruption of data from any partition does not affect the other partitions. Furthermore, because compression is progressive within each partition, when data are lost, any data from that partition received prior to the loss can be used to reconstruct that partition at lower fidelity.

By virtue of the compression improvement it achieves relative to previous means of onboard data compression, this software enables (1) increased return of hyperspectral scientific data in the presence of limits on the rates of transmission of data from spacecraft to Earth via radio communication links and/or (2) reduction in spacecraft radio-communication power and/or cost through reduction in the amounts of data required to be downlinked and stored onboard prior to downlink. The software is also suitable for compressing hyperspectral images for ground storage or archival purposes.

*This program was written by Hua Xie, Aaron Kiely, Matthew Klimesh, and Nazeeh Aranki of Caltech for NASA's Jet Propulsion Laboratory.*

*This software is available for commercial licensing. Please contact Karina Edmonds of the California Institute of Technology at (626) 395-2322. Refer to NPO-43238.*

## Context Modeler for Wavelet Compression of Spectral Hyperspectral Images

A context-modeling subalgorithm has been developed as part of an algorithm that effects three-dimensional (3D) wavelet-based compression of hyperspectral image data. The context-modeling subalgorithm, hereafter denoted the context modeler, provides estimates of probability distributions of wavelet-transformed data being encoded. These estimates are utilized by an entropy coding subalgorithm that is another major component of the compression algorithm. The estimates make it possible to compress the image data more effectively than would otherwise be possible.

The following background discussion is prerequisite to a meaningful summary of the context modeler. This discussion is presented relative to “ICER-3D,” which is the name attached to a particular compression algorithm and the software that implements it. The ICER-3D software is summarized briefly in the preceding article, “ICER-3D Hyperspectral Image Compression Software” (NPO-43238). Some aspects of this algorithm were previously described, in a slightly more general con-

text than the ICER-3D software, in “Improving 3D Wavelet-Based Compression of Hyperspectral Images” (NPO-41381), *NASA Tech Briefs*, Vol. 33, No. 3 (March 2009), page 7a. In turn, ICER-3D is a product of generalization of ICER, another previously reported algorithm and computer program that can perform both lossless and lossy wavelet-based compression and decompression of gray-scale-image data.

In ICER-3D, hyperspectral image data are decomposed using a 3D discrete wavelet transform (DWT). Following wavelet decomposition, mean values are subtracted from spatial planes of spatially low-pass subbands prior to encoding. The resulting data are converted to sign-magnitude form and compressed. In ICER-3D, compression is progressive, in that compressed information is ordered so that as more of the compressed data stream is received, successive reconstructions of the hyperspectral image data are of successively higher overall fidelity.

Before encoding each bit, the probability that the bit is a zero is estimated. The probability-of-zero estimate relies only on previously encoded information. The bit and its probability-of-zero estimate are sent to the entropy coding subalgorithm (hereafter denoted the entropy encoder), which effects the desired compression of the sequence of bits that it receives. Better probability-of-zero estimates allow the entropy coder to achieve better data compression. It is the job of the context modeler to produce these probability-of-zero estimates. This concludes the background discussion.

In the context modeling subalgorithm, a bit of a DWT coefficient to be encoded is first classified into one of 19 contexts based on the values of previously encoded bits. Each context amounts to a class for which separate probability-of-zero statistics are gathered. ICER-3D employs a one-dimensional spectral-context model involving context definitions that rely on two neighbors in the spectral direction but no neighbors in the same spatial plane. For comparison, ICER uses a two-dimensional context model relying on eight spatial-frequency-domain neighbors.

During the encoding process, DWT coefficients are assigned to categories in preparation for assigning them to contexts. There are four categories, numbered 0 – 3. The category of a coefficient

is initially 0 and remains 0 so as long as the magnitude bits encoded for the coefficient are all zeros. After the first “1” bit from the coefficient is encoded, the category of the coefficient becomes 1. When the next magnitude bit of the coefficient is encoded, its category becomes 2. When one more magnitude bit from the coefficient is encoded, its category becomes 3 and remains 3 permanently. The

context of a bit is determined from the category of the DWT coefficient that contains the bit and the category and signs of the two neighboring coefficients in the spectral dimension.

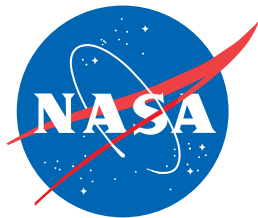
Compared to the 2D context model used by ICER, the ICER-3D context modeler provides noticeable improvement in compression of sign bits and bits in category 0, and slight improve-

ment for the other categories of bits that are compressed.

*This work was done by Aaron Kieley, Hua Xie, Matthew Klimesh, and Nazeeh Aranki of Caltech for NASA's Jet Propulsion Laboratory.*

*The software used in this innovation is available for commercial licensing. Please contact Karina Edmonds of the California Institute of Technology at (626) 395-2322. Refer to NPO-43239.*





National Aeronautics and  
Space Administration